Journal of Medicinal Chemistry

Article

Induced Fit in Mouse Acetylcholinesterase upon Binding a Femtomolar Inhibitor: A Molecular Dynamics Study

Sanjib Senapati, Jennifer M. Bui, and J. Andrew McCammon

J. Med. Chem., **2005**, 48 (26), 8155-8162• DOI: 10.1021/jm050669m • Publication Date (Web): 22 November 2005

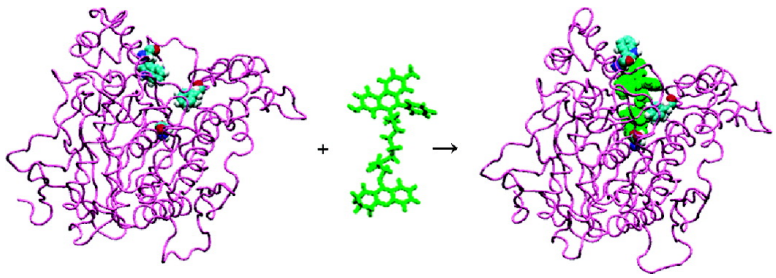

More About This Article

Additional resources and features associated with this article are available within the HTML version:

- Supporting Information
- Links to the 5 articles that cite this article, as of the time of this article download
- Access to high resolution figures
- Links to articles and content related to this article
- Copyright permission to reproduce figures and/or text from this article

View the Full Text HTML

Journal of Medicinal Chemistry is published by the American Chemical Society. 1155 Sixteenth Street N.W., Washington, DC 20036

Induced Fit in Mouse Acetylcholinesterase upon Binding a Femtomolar Inhibitor: A Molecular Dynamics Study

Sanjib Senapati,*,† Jennifer M. Bui,† and J. Andrew McCammon†,‡,§

Department of Chemistry and Biochemistry, University of California, San Diego, La Jolla, California 92093-0365, Howard Hughes Medical Institute, University of California, San Diego, La Jolla, California 92093-0365, and Department of Pharmacology, University of California, San Diego, La Jolla, California 92093-0365

Received July 14, 2005

A molecular dynamics simulation of mouse acetylcholinesterase (mAChE) complexed with *syn*-TZ2PA6, a femtomolar AChE inhibitor, is compared to a simulation of unliganded mAChE. The simulation of the complex was initiated by placing the inhibitor in its bound conformation of the crystal complex into a structure of unliganded mAChE selected from preliminary protein−ligand docking results. During a 2 ns period, the enzyme subsequently displayed a substantial "induced fit" response to yield a conformation very similar to that obtained by crystallography (Bourne et al. *Proc. Natl. Acad. Sci. U.S.A.* **2004**, *101*, 1449−1454). In this conformation of unique nature, the Trp 286 side chain of the enzyme flips out of the hydrophobic core and becomes highly solvent exposed. The imidazole ring of His 287 is almost orthogonal relative to its position in the unliganded enzyme, creating a stable π stacking arrangement with the Trp 286 side chain. Other major deviations among the active site residues include side chain conformational changes of Trp 86, Tyr 133, Tyr 337, and Phe 338. These residues in the complex deviate from their positions in unliganded mAChE to better accommodate the inhibitor in the active site gorge.

Introduction

The mechanism of enzyme catalysis/inhibition begins with the binding of the substrate or inhibitor to the active site pocket on the enzyme. The substrate might bind in a reactive orientation of the enzyme in a lock-and-key fashion, or it may distort the enzyme on binding, making the resulting complex more susceptible to bond making/breaking.[2] The "lock and key" concept for enzyme−substrate interactions is inadequate to explain all experimental examples of enzyme reactivity. The later postulate known as "induced fit" has, therefore, been proposed. It assumes that the substrate plays a role in determining the final shape of the enzyme. In this work, combining protein−ligand docking results with molecular dynamics (MD) simulations, we capture one such "induced fit" response in mAChE and have shown that our results complement the experimental observations. We note that, in future work, one should additionally consider the considerable conformational flexibility of the complicated ligand studied in this work in its unbound and complexed forms.

The enzyme we have chosen to study is AChE, a serine hydrolase responsible for the termination of impulse signaling at cholinergic synapses.[3] It catalyzes the hydrolysis of the neurotransmitter acetylcholine (ACh) into acetate and choline.[4] It is an extremely effective catalyst, acting at nearly diffusion-controlled rates to terminate the action of ACh on postsynaptic receptors. The active site of AChE is located at the base of a long and narrow 20 Å gorge. It consists of an esteratic subsite containing the catalytic machinery and an anionic subsite responsible for binding the quaternary trimethylammonium tailgroup of ACh.[5] The essential catalytic functional unit of AChE is the catalytic triad consisting of Ser 203, His 447, and Glu 334. The oxyanion hole, formed by the peptidic NH groups of Gly 121, Gly 122, and Ala 204, is another important functional unit in the esteratic subsite. The anionic subsite consists of residues Trp 86, Glu 202, and Tyr 337. The peripheral anionic site (PAS) located at the rim of the active center gorge[6,7] and composed of surface residues Tyr 72, Trp 286, and His 287 plays an important role in binding the allosteric inhibitors. Besides the gorge, MD simulations of mAChE showed a couple of alternative portals providing access to the catalytic site in AChE. These openings, named the side channel and the back door, may facilitate rapid solvent and product removal.[8−10] While the side channel is formed by the residues Thr 75, Leu 76, and Thr 83, the back door is composed of Trp 86, Gly 448, Tyr 449, and Ile 451.

The inhibitor of our interest is *syn*-TZ2PA6, a triazole regioisomer of TZ2PA6 in syn conformation (Figure 1). It is an ultra-high-affinity inhibitor of AChE,[1,11−13] produced in situ from precursor fragments by "click chemistry". The dissociation constants (K_d) of *syn*-TZ2PA6 of 77 to 410 fM were found, depending on the species, which makes it the most potent noncovalent AChE inhibitor known to date by approximately 2 orders of magnitude.[11] AChE inhibitors have been used for over a century in various therapeutic regimens.[4,14] The crystal structure of *syn*-TZ2PA6 complexed with mouse AChE (mAChE) has become available very recently.[1] This study has revealed that the enzyme in the complex attains a conformation where its Trp 286

* To whom correspondence should be addressed. E-mail: ssenapat@mccammon.ucsd.edu, Ph.: 858-822-0169, Fax: 858-534-4974.
† Department of Chemistry and Biochemistry.
‡ Howard Hughes Medical Institute.
§ Department of Pharmacology.

10.1021/jm050669m CCC: $30.25
Published on Web 11/22/2005

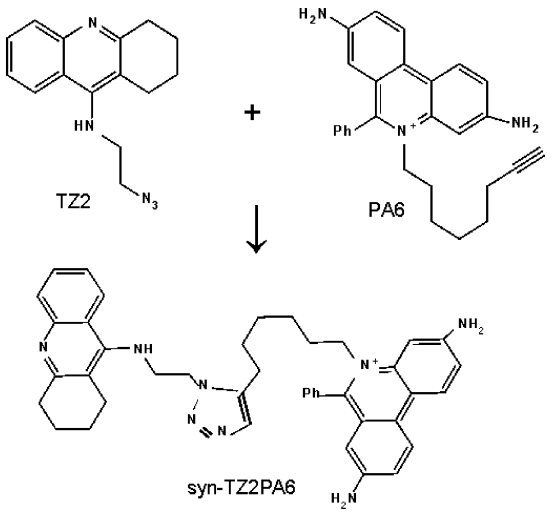

Figure 1. Structure of the *syn*-TZ2PA6 inhibitor formed by 1,3-dipolar cycloaddition. The tacrine, triazole, and phenylphenanthridinium moieties are shown from left to right.

side chain is displaced from the AChE hydrophobic core toward the solvent. Our simulation data not only complement this experimental finding but also provide an insight into the internal motions of the enzyme on an atomic level. A MD simulation of unliganded mouse AChE is also performed to detect differences and similarities of structural transitions and dynamic fluctuations of residues upon complexation and to compare the solvation properties of the surface residues at the peripheral anionic site.

Preparation of the Systems

Our study started with an automated docking of *syn*-TZ2PA6 to a large ensemble of MD snapshots of *apo*-mAChE, following a novel computational approach for drug design, called the "relaxed-complex" method,[15,16] which allows for the direct accommodation of the receptor's flexibility. AutoDock 3.0.5[17] was adopted in the "relaxed-complex" scheme to perform an efficient docking of large, flexible ligands. We found that *syn*-TZ2PA6 does not fit into the binding pocket of the apoform of the enzyme. Although one of its precursor reactants, TZ2 (Figure 1), can be accommodated nicely at the bottom of the active center gorge (practically superimposed on tacrine in the crystal structure of *syn*-TZ2PA6-mAChE complex), the PA6 fragment or phenanthridinium moiety makes strong steric clashes with the PAS residues (Figure 2). Thus, the inhibitor does not bind to the enzyme in a lock-and-key fashion. To check if *syn*-TZ2PA6 can fit into the protein gorge by a induced fit response of the receptor, we carried out a MD simulation of *apo*-mAChE bound to *syn*-TZ2PA6.

A snapshot of *apo*-mAChE with a large gorge opening that was capable of accommodating TZ2 nicely during the docking studies (i.e. docked TZ2 practically superimposed on tacrine in the crystal structure) was chosen as the starting configuration for the MD simulation. The setup for the unliganded simulation has been described in the previous paper[18] and is summarized here. The 3.2 Å crystal structure of Fas2-mAChE (PDB identification code 1MAH[19]) was used to build a model of unliganded AChE. Fasciculin was deleted from the structure, and the coordinates of missing residues Pro

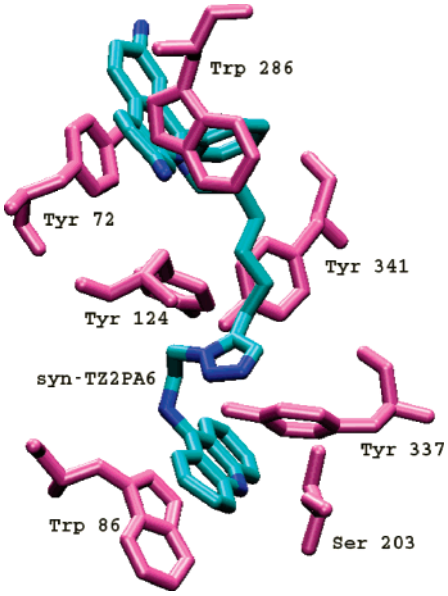

Figure 2. A blow-up figure of the starting conformation of the *syn*-TZ2PA6−mAChE complex in our simulation. The position of the ligand along with a few active site residues are displayed. The hydrogen atoms are omitted for clarity. The ligand is colored by atom type: cyan, C; blue, N; and the protein residues are colored pink.

258, Pro 259, Gly 260, Gly 261, Ala 262, Gly 263, Gly 264 and for the missing side chains of Arg 253, Arg 364, Arg 470, Asp 491, and Lys 496 were modeled using the InsightII graphics package.[20]

It is known that the buried waters in the active site gorge play an important role in ligand binding.[21] Therefore, the crystal water molecules in the 1MAH structure were generated in the following way.[8] Favorable locations in the protein that might contain waters were determined using the GRID program,[22] which calculates the interaction of a water probe with the protein on a fine grid. For any cavity with a potential energy less than −46 kJ/mol, a water molecule was placed in that position if it could make at least two hydrogen bonds. In larger cavities, two water molecules were placed. Bump checks were performed on the structure to ensure waters were not too close to the protein.

The WHATIF program[23] was used to optimize the hydrogen bond network of the starting configuration, which involved rotatable protein hydroxyl side chains and crystal water molecules. InsightII was used to add the remaining hydrogens to the structure. Added hydrogens were energy minimized for 100 steps using the steepest descent algorithm.

A set of partial atomic charges of the ligand was obtained via quantum electronic structure calculations. Using the Gaussian 98 program[24] with the 6-31G* basis set, we performed a Hartree−Fock geometry optimization procedure. The atom-centered RESP charges were determined via fits to the electrostatic potentials obtained from the calculated wave functions. The missing interaction parameters in the ligand were generated using antechamber tools in Amber.[25] The ligand coordinates in the starting configuration were obtained by the following procedure. The crystal structure of *syn*-TZ2PA6-mAChE[1] complex was superimposed onto the selected *apo*-AChE starting configuration. The trans-

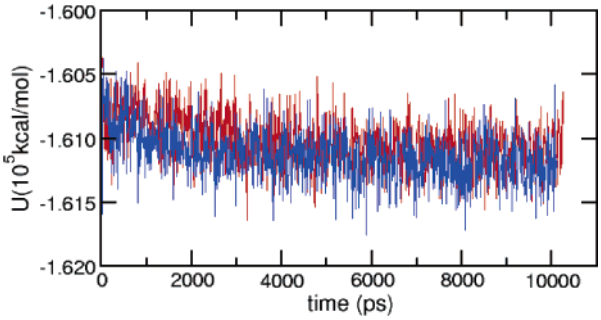

Figure 3. The behavior of the instantaneous potential energy for the unliganded (red) and liganded simulation (blue).

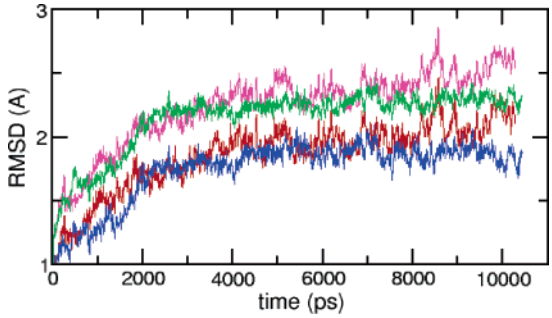

Figure 4. Time dependence of the root-mean-square deviations for the 10-ns MD trajectories. Red for CA atoms of *apo*-mAChE, blue for CA atoms of mAChE complexed with *syn*-TZ2PA6, pink for heavy atoms of *apo*-mAChE, and green for heavy atoms of mAChE complexed with *syn*-TZ2PA6.

formed ligand coordinates from the crystal structure were then incorporated into the *apo*-AChE coordinate file. We acknowledge that this modeling procedure requires prior knowledge about the crystal structure of the bound complex. It is therefore not applicable for de novo prediction of the binding modes of such complex ligands to AChE.

The enzyme, in both the systems, was solvated in a cubic box of water of 90 Å in length. Ten sodium ions (nine in case of the complex simulation, as the ligand has charge +1) were placed in the solvent randomly to neutralize the −10 charge of the protein. For the complex simulation, a set of minimization and thermalization runs of the starting structure was performed keeping the tacrine moiety of the ligand fixed to remove the initial strain. A 500 ps equilibration run in the NPT ensemble was then conducted, this time letting the tacrine moiety go free. This last simulation provided the initial conditions for the production run of 10 ns in the NVT ensemble. The unliganded system was also equilibrated for 500 ps at 300 K in NPT ensemble, and the final conformations of the protein were collected from a 10 ns production run in NVT ensemble.

All minimization and MD steps were performed using the NAMD package[26] with Amber force fields.[27] Particle-Mesh Ewald summation[28] with a 10 Å short-range cutoff was used to treat long-range electrostatics. SHAKE was used to constrain bond lengths between heavy atoms and hydrogens. The time step used was 2 fs, and the system pressure was restrained to 1 atm, with a coupling time of 0.4 ps. The calculations were performed on 8 processors of Xeon 2.8 GHz linux cluster, and each 10 ns simulation took about 8 processor-months to finish.

Results and Discussion

It is always necessary to ensure that the system has been reasonably equilibrated before starting the production run. A simple way to monitor system equilibration is to record the instantaneous values of the potential energy during this period. The behavior of the instantaneous potential energy for both the systems is shown in Figure 3. This figure shows that the potential energies of the systems have ceased to show a systematic drift at around 2 ns of the simulations and then have started to oscillate about steady mean values. The initial drift is expected as the protein residues reduce any unfavorable interactions and the solvent molecules relax around them.

An additional strategy involves monitoring the mean squared displacements of residues from their initial positions. This function increases during the initial phase of the simulation but oscillates around a mean value in the later phase. Figure 4 shows the rms deviations (rmsd) of the CA and heavy atoms of the protein compared to their corresponding positions in the initial structure for both the liganded and unliganded simulations. This figure again shows convergence of rms deviations at approximately 2 ns. A relatively long convergence time is not unexpected considering the big size of the system. After the convergence, the average deviation is about 1.8 Å for CA atoms in both the systems. The average deviation for the heavy atoms is somewhat larger and is about 2.3 Å. We note that the rms deviations for the apo-enzyme are increasing slightly near the end of the 10 ns trajectory. However, this is not a major issue that may impact the system stability. The temperature, the total energy, the mass density, the volume, and the energy components of the system were inspected to ensure the stability of the trajectory.

We note that during the 2 ns convergence process the protein structure in the complex simulation has undergone "induced fit" conformational changes to better accommodate the inhibitor in the active site gorge. The side chains of the PAS residues deviate significantly to avoid the steric clash with the phenylphenanthridinium moiety of the ligand (Figure 2). The side chains of the other active site residues reorient themselves according to the position and orientation of the triazole and tacrine moieties in the ligand. This leads to a conformation of the protein that remains stable throughout the later phase of the simulation run and resembles the X-ray structure[1] very closely.

Figure 5 shows a comparison between the two structures of the *syn*-TZ2PA6-mAChE complex. In a close-up view only the structures of the bound ligand along with a few active site residues are displayed. The protein residues and the ligand from the crystallographic data are colored yellow. The structures from the simulation are colored according to atom type: cyan, C; red, O; blue, N. The hydrogen atoms are not shown for clarity. This figure was generated by a stereo superposition of the crystal structure of the complex and the average structure of the same from simulation, according to all atoms of mAChE. The average structure from simulation was obtained by superposing the enzyme conformations onto that in the starting structure and taking the mean of the atom positions at every 10 ps interval during the last 8 ns run. This figure clearly

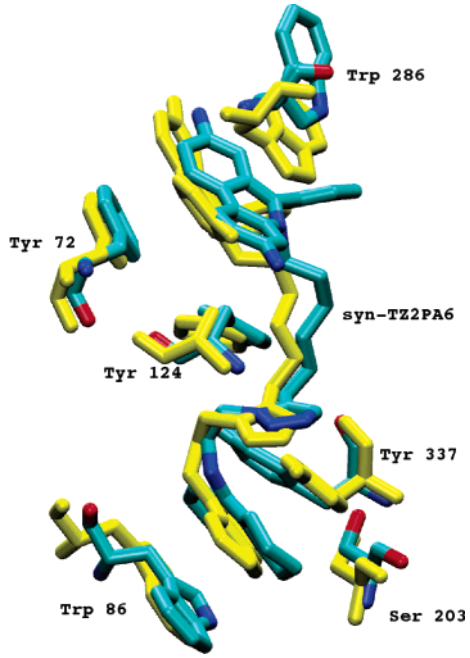

Figure 5. A close-up view of the *syn*-TZ2PA6-mAChE complex from X-ray data (yellow) and MD simulation (colored by atom type: cyan, C; red, O; blue, N). The position of the bound ligand along with a few active site residues are displayed. The hydrogen atoms are omitted for clarity. The figure is generated by a stereo superposition of the crystal structure and the average structure from simulation according to all atoms of mAChE.

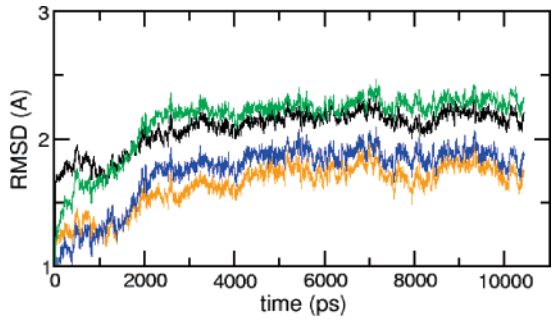

Figure 6. Time dependence of the root-mean-square deviations of the C-alpha and heavy atoms of the protein in *syn*-TZ2PA6-mAChE complexes. Yellow: C-alpha atoms from X-ray structure, blue: C-alpha atoms from starting structure in the simulation, black: heavy atoms from X-ray structure, green: heavy atoms from starting structure in the simulation.

shows that the inhibitor in the simulation deviates very slightly from its original conformation and gets stabilized in the gorge by inducing conformational changes to the adjacent protein residues. The resultant protein structure is very similar to the X-ray structure. The relative deviations and fluctuations of the protein residues from the *apo*-AChE simulation are discussed in the following paragraphs.

We have computed the rms deviations of the CA and heavy atoms of the protein, taking the X-ray structure of the *syn*-TZ2PA6−mAChE complex as the reference structure. The results are presented in Figure 6. The rms deviations from the starting configuration of the liganded simulation are also plotted for comparison. This figure shows that the rms deviations are smaller when the X-ray structure is taken as the reference, especially after 2 ns of simulation run. The 0.5 and 1.3

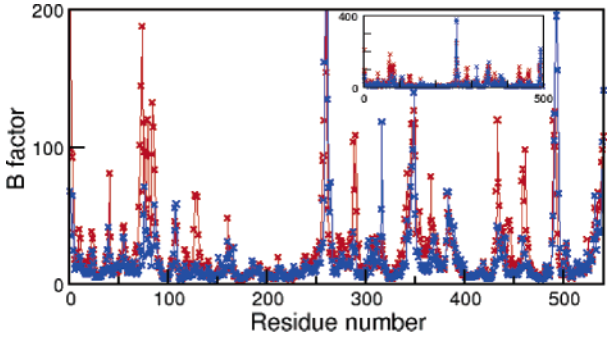

Figure 7. The *B* factor for each residue in both the systems. Red for residues in *apo*-mAChE and blue for residues in mAChE complexed with *syn*-TZ2PA6. Inset displays the largest *B*-factor values.

Å of rmsd at the starting point are due to the difference between the two reference structures. Subtracting these values as the baseline, the actual rmsd due to MD are even smaller than those shown in Figure 6. This again indicates that the protein in our complex simulation transforms to a conformation that is similar to the ones observed in the crystal structure.

After noting that the enzyme in our complex simulation has undergone structural changes, we then proceed to compare these changes with respect to the simulation results from the unliganded simulation. Note that both the systems were simulated under the same state conditions. The results of structural transitions and dynamic fluctuations of protein residues upon complexation are presented below.

To identify the relative internal motions of the protein residues in the two simulations, we calculate the isotropic temperature (B) factor. This quantity can be calculated from the mean square fluctuation (msf) using the following equation:[29]

$$B = \frac{8\pi^2}{3}(\text{msf}) \qquad (1)$$

The B factor plots for each residue from the msf in the simulations are presented in Figure 7. This has revealed the complex nature of the fluctuations of the protein residues. Residues Thr 75, Leu 76, and Thr 83 that comprise the side channel[9,8] show reduced flexibility upon complexation. The back door passage,[10] bounded by residues Trp 86, Tyr 449, and Ile 451, also shows a reduced flexibility in the complex. The aromatic ring of Tyr 133 (another active site residue) is found to rotate by about 90° in the complex, which facilitates stable bonding between Tyr 133: OH and Trp 117: NE1. This has led to smaller fluctuations of these residues in the complex, as can be seen from Figure 7. Residues 291−297 that are either in the active site or close to it also show smaller flexibility in the complex. This can be explained as a direct interaction of these residues with the inhibitor. For example, OE1 and OE2 of Glu 292 form hydrogen bonds with the NH_2 group of phenylphenanthridinium moiety in the ligand. Glu 292: O also interacts with the phenyl π-system of this moiety. Ser 293: O and Ile 294: N may also interact with the phenyl π-system from the other side of the plane of the ring. This chain of residues in the complex deviates significantly compared to the unliganded structure and aligns in a way that best fits the tail region of the

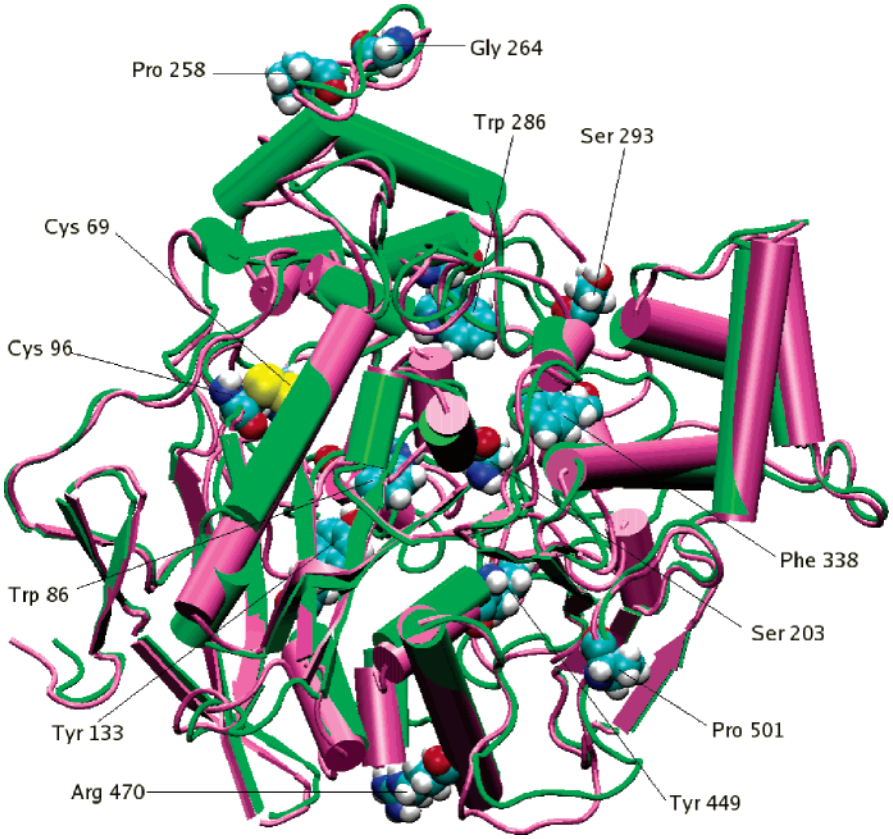

Figure 8. The average structure of the unliganded protein (pink) and that of the protein in the complex (green). The location of a few residues in the unliganded mAChE are shown in space-filling representation. The figure is produced by superposing the average enzyme structures according to all atoms of mAChE.

inhibitor in the PAS. Most of the other active site residues, e.g. Tyr 337, Phe 338, His 447, also show reduced fluctuations upon binding to the ligand. The surface residues Asp 320−Asp 323, however, exhibit increased fluctuations upon complexation. The stable hydrogen bonds between the NH_2 group of Gln 322 and Asp 320: OD1, OD2 (in the unliganded simulation) become intermittent hydrogen bonds in the complex. Other surface residues 259−267, 344−353, 463−470, and 495−501, as expected show the highest fluctuations. Except for the residues 463−470, the fluctuation is always higher in the complex. This is hard to explain, as the surface fluctuations result in part from a competition between interresidue and water-mediated hydrogen bonding. Overall, the liganded simulation shows smaller structural deviations and fluctuations, particularly of the active site residues. This can be explained as the result of stabilizing interactions of the ligand moieties with these residues.

We then compare the average structures of the enzyme for the apo and the complex simulations. The average structures are obtained as stated above. The resulting two average structures are shown in Figure 8. While the overall agreement between the two structures is close, there are many places where they differ significantly. An interesting place to look at is the long omega loop defined by the Cys 69−Cys 96 disulfide bond. This loop comprises the thin wall of the active site and has relatively little interaction with other parts of the protein. Within this segment, residues 81−85 may be considered as one turn of an α-helix, and residues 84−87 form a distorted β-turn of intermediate type.[30,31] In our liganded simulation, all these residues are found to display reduced motion. Here, the loop undergoes a much smaller deviation and fluctuation from the starting structure positions (deviation: 2.0 Å; fluctuation: 0.4 Å) compared to the unliganded simulation (deviation: 3.4 Å; fluctuation: 0.7 Å). Note that the fluctuation relates to the mobility of atoms in a residue around their average positions, while the deviation for a residue indicates the displacement of the average atomic positions from the crystal structure positions. This altered motion of the loop narrows the route of access to the active site, which is a direct manifestation of the stabilizing effect of the ligand in the active site. The distal small omega loop[32] (Pro 258−Gly 264) also differs upon binding, though the difference dies down at longer time.

We also looked at the helices 2 and 14 very closely, as they contain the largest number of gorge residues. Helix 2 consists of residues 81−86 and helix 14 contains residues 335−342.[8] It is, therefore, not surprising that these two helices also behave differently in the two simulations. The indole of Trp 86 in the complex flips by about 60° from its average position in the *apo*-AChE and is stacked against the tacrine moiety of the ligand. The aromatic side chain of Tyr 337 in the complex rotates by about 40° and orients itself in such a way that enhances a stacking stabilization of the tetrahydroaminoacridine ring inserted between the Trp 86 and Tyr 337 aromatic side chains, an observation that is in excellent agreement with the reported crystal structure of the complex.[1] The aromatic rings of Tyr 124 and Phe 338 in the constricted region within the gorge also move

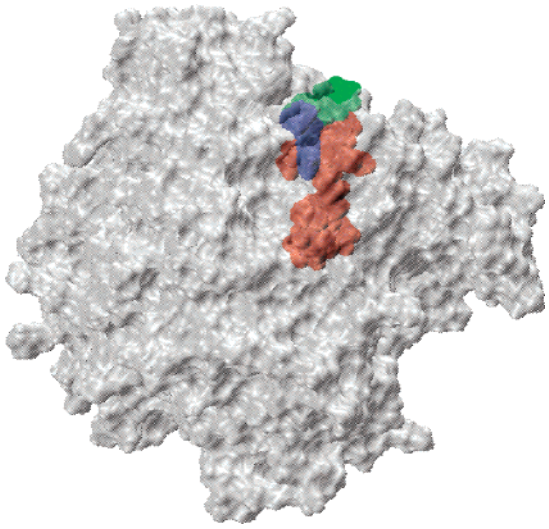

Figure 9. The location of Trp 286 in the complex (green) relative to its location in *apo*-AChE (blue). The position of TZ2PA6 in the complex is shown in red. The brighter region of green color means a completely solvent exposed region, while other shaded regions imply inside or on the surface of AChE. The figure is produced in the same way as described in Figure 8.

to a conformation where they are almost parallel to the triazole moiety of the inhibitor to induce an enhanced stacking stabilization among the aromatic rings in the complex. The Tyr 341 aromatic ring also bends by about 30° and favors a stacking stabilization of the phenyl group of the phenylphenanthridinium moiety in the ligand.

The most striking differences, however, are seen in the peripheral site where the residues are more mobile on the surface of the protein. Here, the Trp 286 side chain in the complex flips out by about 140° from its average position in the *apo*-AChE to avoid the steric clash with the phenylphenanthridinium moiety of the ligand (Figure 9). This causes the Trp 286 side chain in the complex to be well exposed to solvent which creates an opening at the gorge rim that is 2-fold larger (about 7.8 Å) than in the *apo*-AChE. This is an unusual conformation of the protein that is observed only in the presence of *syn*-TZ2PA6 inhibitor and is in excellent agreement with the X-ray structure of the complex.[1]

We have quantitatively measured the extent of solvation of the Trp 286 side chain due to complexation. We define the hydration number of the Trp 286 side chain as the measure for the extent of solvation. We determine the average hydration number of the Trp 286 side chain by counting the number of water molecules in the first solvation shell of the Trp 286 side chain. We noticed a substantial overlap between the solvation shells of two adjacent atoms in the same chain. Therefore, while calculating the solvation number, we counted each water molecule in the first solvation shell just once. Figure 10 displays the time evolution of the solvation number for both the systems. As is clear from this figure, except for the initial phase which is required for the Trp 286 side chain to flip out, the solvation of the Trp 286 side chain in the complex is always higher than that in *apo*-AChE. The average value of the solvation number we got for the Trp 286 side chain in the complex is 12, compared to the value of 6 in *apo*-AChE. Thus,

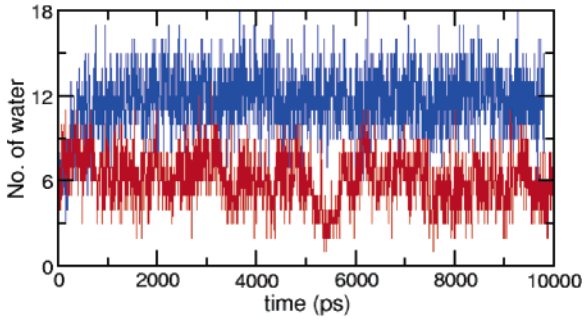

Figure 10. Number of water molecules around the Trp 286 side chain as a function of time. Blue for complex simulation, red for unliganded simulation.

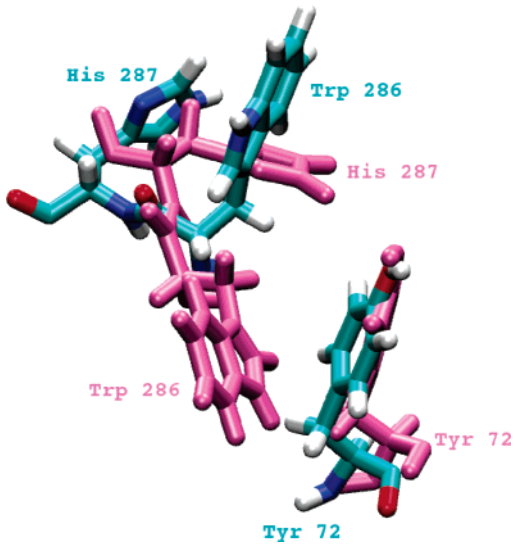

Figure 11. The relative position of a few important PAS residues. Residues in pink are from *apo*-AChE and others are from AChE in complex. Cyan, C; red, O; blue, N; white, H. The figure is produced in the same way as described in Figure 8.

the presence of TZ2PA6 causes a sharp increase in solvation of Trp 286 which was otherwise in the hydrophobic core of the protein.

This flipped conformation of Trp 286, in its turn, induces another interesting conformational change at the PAS. The imidazole ring of His 287 now moves to a conformation where it is almost orthogonal relative to its position in the unliganded protein. This is shown in Figure 11. This figure also shows the locations and orientations of a few other important PAS residues. The Tyr 72 aromatic ring undergoes a slight conformational change. But, His 287 is displaced quite substantially relative to its average position in *apo*-AChE, and now its side chain orients itself in such a fashion that facilitates a parallel $\pi-\pi$ stacking interaction between the aromatic rings of Trp 286 and His 287. We compute the time dependence of χ_2 dihedral angle of His 287 for the entire 10 ns run, and the result is presented in Figure 12. This figure shows that the fluctuation in χ_2 angle of H287 in the complex simulation is much smaller than in the apo-simulation. We also visualize the conformational changes in the protein−inhibitor complex and note that the side chains of Trp 286 and His 287 remain almost parallel to each other, at least after the 2 ns of relaxation. A smaller fluctuation of the His 287 side chain in the complex simulation is again

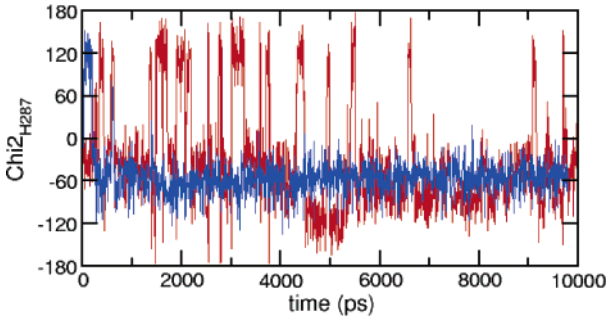

Figure 12. The time evolution of dihedral angle χ_2 (CA−CB−CG−ND1) of His 287. Blue for TZ2PA6-AChE complex, red for *apo*-AChE.

an indication of a stable rearrangement of the PAS residues. We also have calculated the extent of solvation of the His 287 side chain due to this rearrangement. The solvation of the His 287 side chain is found to be smaller in the complex than in the unliganded simulation. The average value of the solvation number is calculated to be 8 in the complex simulation, compared to a value of 11 in *apo*-AChE simulation. This reduced solvation of the His 287 side chain can be explained from the fact that water cannot access one face of the imidazole ring that is involved in near parallel stacking interaction with the indole of Trp 286.

Summary and Conclusions

A molecular dynamics simulation of mouse acetylcholinesterase (mAChE) complexed with *syn*-TZ2PA6 is compared to a simulation of *apo*-mAChE. The simulation of the complex was initiated by placing the inhibitor in its crystallographic binding mode into a structure of the unliganded enzyme selected from preliminary protein−ligand docking results. During a 2 ns period, the protein has undergone "induced fit" conformational changes to attain a structure that is very similar to the one seen in the X-ray structure of the complex. The rest of the structure of the simulated complex during the last 8 ns simulation run remains stable and resembles the X-ray structure of the complex.

The internal motions of the protein residues in both the simulations show a complex nature. Residues that comprise the side channel and back door passages in mAChE show a reduced flexibility upon complexation. The aromatic ring of Tyr 133 is found to rotate by about 90° in the complex, which facilitates stable bonding between Tyr 133: OH and Trp 117: NE1. A reduced motion of the long omega loop in the complex simulation narrows the route of access to the active site. The aromatic moieties of the ligand and the aromatic rings of Trp 86, Tyr 124, Tyr 337, Phe 338, and Tyr 341 reorient themselves in a manner that induces an enhanced stacking stabilization across the active site gorge. Most of the other active site residues also show reduced fluctuations upon binding to the ligand.

In the peripheral anionic site, the side chains of the residues are found to be dislodged upon complexation. The Trp 286 side chain in the complex flips out by about 140° to be well exposed to the solvent. A quantitative estimate of the solvation shows a solvent coordination number that is two times larger than in the unliganded simulation. The imidazole ring of His 287 deviates to a position from where it introduces a stacking stabilization with the indole of Trp 286. Overall, the side chains of the protein residues, particularly those in the active site, deviate from their positions in unliganded mAChE to better accommodate the inhibitor in the complex. These changes in the protein structure can be attributed, in part, to the interaction of the enzyme with the inhibitor.

Acknowledgment. We thank Dr. Zoran Radic, Prof. Hartmuth C. Kolb, Dr. Yves Bourne, Dr. Pascale Marchot, and Prof. Palmer Taylor for providing early access to the crystal structure of the *syn*-TZ2PA6−mAChE complex. J.A.M. thanks Prof. Barry Sharpless for a conversation that stimulated this work. This work was supported in part by NIH, NSF, the Howard Hughes Medical Institute, the National Biomedical Computation Resource, the NSF Center for Theoretical Biological Physics, the W. M. Keck Foundation, and Accelrys, Inc.

References

(1) Bourne, Y.; Kolb, H. C.; Radic, Z.; Sharpless, K. B.; Taylor, P.; Marchot, P. Freeze-frame inhibitor captures acetylcholinesterase in a unique conformation. *Proc. Natl. Acad. Sci. U.S.A.* **2004**, *101*, 1449−1454.
(2) Koshland, D. E., Jr. The Key-Lock Theory and the Induced Fit Theory. *Angew. Chem., Int. Ed. Engl.* **1994**, *33*, 2375−2378.
(3) Kandel, E. R.; Schwartz, J. H.; Jessell, T. M. *Principles of Neural Science*, 3rd ed.; Appleton & Lange, Norwalk, CT, 1991.
(4) Barnard, E. A. In *The Peripheral Nervous System*; Hubbard, J. I., Ed.; Plenum Publishers: New York, 1974; pp 201−206.
(5) Quinn, D. M. Acetylcholinesterase: enzyme structure, reaction dynamics, and virtual transition states. *Chem. Rev.* **1987**, *87*, 955−979.
(6) Radic, Z.; Reiner, E.; Taylor, P. Role of the peripheral anionic site on acetylcholinesterase: inhibition by substrates and coumarin derivatives. *Mol. Pharmacol.* **1991**, *39*, 98−104.
(7) Bourne, Y.; Taylor, P.; Radic, Z.; Marchot, P. Structural insights into ligand interactions at the acetylcholinesterase peripheral anionic site. *EMBO J.* **2003**, *22*, 1−12.
(8) Tara, S.; Straatsma, T. P.; McCammon, J. A. Mouse acetylcholinesterase unliganded and in complex with huperzine A: A comparison of molecular dynamics simulations. *Biopolymers* **1999**, *50*, 35−43.
(9) Wlodek, S. T.; Clark, T. W.; Scott, L. R.; McCammon, J. A. Molecular Dynamics of Acetylcholinesterase Dimer Complexed with Tacrine. *J. Am. Chem. Soc.* **1997**, *119*, 9513−9522.
(10) Gilson, M. K.; Straatsma, T. P.; McCammon, J. A.; Ripoll, D. R.; Faerman, C. H.; Axelsen, P. H.; Silman, J. L. Open "Back Door" in a Molecular Dynamics Simulation of Acetylcholinesterase. *Science* **1994**, *263*, 1276−1278.
(11) Lewis, W. G.; Green, L. G.; Grynszpan, F.; Radic, Z.; Carlier, P. R.; Taylor, P.; Finn, M. G.; Sharpless, K. B. Click Chemistry In Situ: Acetylcholinesterase as a Reaction Vessel for the Selective Assembly of a Femtomolar Inhibitor from an Array of Building Blocks. *Angew. Chem., Int. Ed.* **2002**, *41*, 1053−1057.
(12) Manetsch, R.; Krasinski, Q.; Radic, Z.; Raushel, J.; Taylor, P.; Sharpless, K. B.; Kolb, H. C. In Situ Click Chemistry: Enzyme Inhibitors Made to Their Own Specifications. *J. Am. Chem. Soc.* **2004**, *126*, 12809−12818.
(13) Krasinski, Q.; Radic, Z.; Manetsch, R.; Raushel, J.; Taylor, P.; Sharpless, K. B.; Kolb, H. C. In Situ Selection of Lead Compounds by Click Chemistry: Target-Guided Optimization of Acetylcholinesterase Inhibitors. *J. Am. Chem. Soc.* **2005**, *127*, 6686−6692.
(14) Dunnett, S. B.; Fibiger, H. C. Role of forebrain cholinergic systems in learning and memory: relevance to the cognitive deficits of aging and Alzheimer's dementia. In *Progress In Brain Research*; Cuello, A. C., Ed.; Elsevier: Amsterdam, 1993; Vol. 98, pp 413−420.
(15) Lin, J.; Perryman, A. L.; Schames, J. R.; McCammon, J. A. Computational Drug Design Accommodating Receptor Flexibility: The Relaxed Complex Scheme. *J. Am. Chem. Soc.* **2002**, *124*, 5632−5633.
(16) Lin, J.; Perryman, A. L.; Schames, J. R.; McCammon, J. A. The Relaxed Complex Method: Accommodating Receptor Flexibility for Drug Design with an Improved Scoring Scheme. *Biopolymers* **2003**, *68*, 47−62.
(17) Morris, G. M.; Goodsell, D. S.; Halliday, R. S.; Huey, R.; Hart, W. E.; Belew, R. K.; Olsen, A. J. Automated Docking Using a Lamarckian Genetic Algorithm and an Empirical Binding Free Energy Function. *J. Comput. Chem.* **1998**, *19*, 1639−1662.

(18) Tai, K.; Shen, T.; Borjesson, U.; Philippopoulos, M.; McCammon, J. A. Analysis of a 10-ns Molecular Dynamics Simulation of Mouse Acetylcholinesterase. *Biophys. J.* **2001**, *81*, 715−724.
(19) Bourne, Y.; Taylor, P.; Marchot, P. Acetylcholinesterase inhibition by fasciculin: Crystal structure of the complex. *Cell* **1995**, *83*, 503−512.
(20) *InsightII*, Accelrys Inc.: San Diego, CA, 1996.
(21) Koellner, G.; Kryger, G.; Millard, C. B.; Silman, I.; Sussman, J. L.; Steiner, T. Active-site gorge and buried water molecules in crystal structures of acetylcholinesterase from Torpedo californica. *J. Mol. Biol.* **2000**, *296*, 713−735.
(22) Goodford, P. J. A computational procedure for determining energetically favorable binding sites on biologically important macromolecules. *J. Med. Chem.* **1985**, *28*, 849−857.
(23) Vriend, G. WHAT IF: A molecular modeling and drug design program. *J. Mol. Graph.* **1990**, *8*, 52−56.
(24) Frisch, M. J. et al. *Gaussian 98, revision A.6;* Gaussian Inc.: Pittsburgh, PA, 1998.
(25) Wang, J.; Cieplak, P.; Kollman, P. A. How well does a restrained electrostatic potential (RESP) model perform in calculating conformational energies of organic and biological molecules? *J. Comput. Chem.* **2000**, *21*, 1049−1074.
(26) Kale, L.; Skeel, R.; Bhandarkar, M.; Brunner, R.; Gursoy, A.; Krawetz, N.; Phillips, J.; Shinozaki, A.; Varadarajan, K.; Schulten, K. NAMD2: Greater Scalability for Parallel Molecular Dynamics. *J. Comput. Phys.* **1999**, *151*, 283−312.
(27) Cornell, W. D.; Cieplak, P.; Bayly, C. I.; Gould, I. R. A Second Generation Force Field for the Simulation of Proteins, Nucleic Acids, and Organic Molecules. *J. Am. Chem. Soc.* **1995**, *117*, 5179−5197.
(28) Darden, T.; York, D.; Pedersen, L. Particle mesh Ewald: An N-log(N) method for Ewald sums in large systems. *J. Chem. Phys.* **1993**, *98*, 10089−10092.
(29) McCammon, J. A.; Harvey, S. *Dynamics of Proteins and Nucleic Acids*; Cambridge University Press: Cambridge, UK, 1987.
(30) Axelsen, P. H.; Harel, M.; Silman, I.; Sussman, J. L. Structure and dynamics of the active site gorge of acetylcholinesterase: Synergistic use of molecular dynamics simulation and X-ray crystallography. *Protein Sci.* **1994**, *3*, 188−197.
(31) Shi, J. X.; Tai, K.; McCammon, J. A.; Taylor, P.; Johnson, D. A. Nanosecond Dynamics of the Mouse Acetylcholinesterase Cys69-Cys96 Omega Loop. *J. Biol. Chem.* **2003**, *278*, 30905−30911.
(32) Tai, K.; Shen, T.; Henchman, R. H.; Bourne, Y.; Marchot, P.; McCammon, J. A. Mechanism of Acetylcholinesterase Inhibition by Fasciculin: A 5-ns Molecular Dynamics Simulation. *J. Am. Chem. Soc.* **2002**, *124*, 6153−6161.

JM050669M